Experimental investigation of geometry effects and performance of five-hole probe in measuring jets in crossflow

Konstantinos Magkoutas*, *Theofilos* Efstathiadis†, and *Anestis* Kalfas‡

AUTh, Department of Mechanical Engineering, Laboratory of Fluid Mechanics and Turbomachinery, Thessaloniki 54124, Greece

Abstract. Vortical and shear flows are common in turbomachinery. Multi-hole pressure probes are used in turbomachinery flows in order to provide robust and accurate measurements of both pressure and velocity components. In this study, two different miniature five-hole probes are designed and fabricated, both with a cobra shape. The probe tip was 1.45 mm and it was maintained in that size for the length of the cobra shape formation, providing very close proximity to the solid boundaries and reduced flow blockage. The difference among the probes corresponded to the head geometry, as the one probe was formed with a pyramid tip shape, while the other was maintained with a flat shape. The calibration process was carried out in an open-circuit suction wind tunnel for the range of ±32º in yaw and pitch direction. The results showed that the pyramid probe exhibits a high flow angle spatial sensitivity and a reliable measurement range of ±28º in yaw and pitch direction. The flat probe provided unexpected well angle sensitivity and reliable measurements data despite the fact that it is of a very simple form. The pyramid probe showed superior performance. In particular, the pyramid probe offers 12.5% wider operating range. In order to prove the effectiveness of the pyramid probe, measurements were obtained in a jet in cross flow. In order to evaluate the performance of the probe, further, a surface fit model was employed to produce ideal calibration coefficients. These were used to redefine the magnitude of the velocities in the measured flow domain. The accuracy in measurements was assessed, comparing the velocities produced by the two variants of pressure coefficients. The results indicate that the pyramid probe operates reliably in a very large range of constantly changing velocity vector, which occurs in jet in cross flow.

Nomenclature

Symbols

C_p non-dimensional pressure coefficient
OD outer stainless steel tube diameter
ID inner stainless steel tube diameter
$D_k$probe's tip diameter
K_{yaw} yaw angle calibration coefficient
K_{pitch} pitch angle calibration coefficient
K_t total pressure calibration coefficient
K_s static pressure calibration coefficient
S_φ yaw sensitivity coefficient
S_γ pitch sensitivity coefficient
V_{jet} injected jet velocity
V_∞ freestream velocity
R velocity ratio (V_{jet}/V_∞)
R^2 coefficient of determination

Greek

φ yaw angle
γ pitch angle

1 Introduction

The multi-hole pressure probes are robust and reliable measurement tools that can obtain simultaneously the magnitude of all three components of the velocity vector, as well as both total and static pressure distributions. Therefore, they are commonly used in turbomachinery and industrial applications when the three dimensional flow field is to be measured. Even though pressure probes with one [1] and seven or more holes are recently developed [2,3], five-hole probes are considered as the most useful means for research in such fields. They

* *Konstantinos* Magkoutas: magkoutk@ethz.ch
† *Theofilos* Efstathiadis: theofil@auth.gr
‡ *Anestis* Kalfas: akalfas@auth.gr

provide sufficient 3Dmeasurements combined with small dimensions, appropriate for complex geometries and facilities with area limitations [4].

Significant efforts have been devoted in devoloping pneumatic pressure probes since their introduction in the 1950s. Dominy and Hodson [5] studied the effects of Reynolds number, Mach number and turbulence intensity on the calibration of various sting probe geometries, for the Reynolds numbers in range between 7 x 10^3 and 8 x 10^4. They found the existence of two distinct Reynolds number effects. One of them is a flow separation around the probe head at relatively low Reynolds numbers when the probe is at incidence. The other is related to changes in the detailed structure of the flow around the sensing holes even when the probe is nulled. These effects were also noticed in the work conducted by Lee and Jun [6], were both yaw and pitch angle altered to cover the full calibration range. Wall proximity and interaction of probe with passage flow are effects of specific interest for turbomachinery applications that have also been studied [7,8]. Chasoglou et al. [9], in a recent study investigated parametrically different geometrical factors that influence the performance of four- and five-hole stem probes.

Although the published work regarding the performance of multi-hole pressure probes, as well as techniques of improving the calibration and data processing methods [10-12] is sufficient, the available studies concerning the fabrication of such probes are rare. Among the first researchers who obtained measurements with miniature five-hole pressure probes were Treaster and Houtz [13]. This study describes the fabrication, calibration and employment of 5-hole probes with tip diameters ranging from 1.07 mm to 1.68 mm. Afterwards, Richards and Johnson [14] in order to obtain measurements of the secondary flowfield developed downstream of the stator blades of a model turbine, employed a miniature five-hole probe with a tip diameter of 1.5 mm. Allen et al. [15] discuss the fabrication and calibration of a MEMSbased five-sensor probe, Georgiou and Milidonis [16] describe a sub-miniature 5-hole probe with embedded pressure sensors for use in extremely confined and complex flow areas in turbomachinery research facilities, while Telionis and Rediniotis [17] review extensively the developments in multihole probes technology as well as examples of their applications.

Recently developed additive manufacturing methods have gained a lot of ground in widening the design space of probe head geometry. Jarallah and Kanjirakkad [18] and Vouros [19], applied multi-jet modelling prototyping methods with wax-based support materials and proposed a

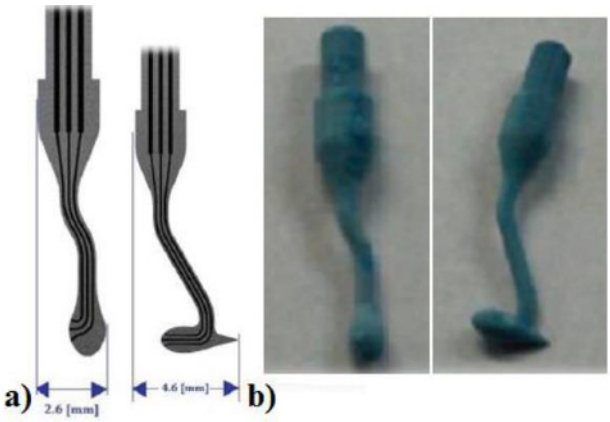

Fig. 1. a) Designed and b) Fabricated head prototypes of stem and sting pressure probes produced using additive manufacturing [19]

viable procedure to manufacture geometrically accurate pneumatic probes (Fig. 1). A common difficulty associated with this manufacturing approach is the effective removal of the supporting material from the long holes, required for multi-hole probes. The problem naturally intensifies when a complex internal geometry design is to be manufactured. Furthermore, the fragile behaviour of materials used in additive manufacturing is a characteristic drawback of the technique compared to the proven fabrication process of the using stainless steel tubing, which can be bend to shape. A number of issues remain to be resolved which make additive manufacturing impractical, at the present time. It is foreseen however, that additive manufacturing may overcome these issues in the near future.

In the current study the fabrication and calibration method of two miniature dimensions five-hole pressure probes are described. Both probes are of cobra shape with tip diameter of 1.45 mm and different head geometry, allowing the effects in probes' performance to be assessed through calibration process. One of the constructed probes was employed in the measurements of jet in cross flow in order to illustrate the probe effectiveness and identify the feasibility of measuring flow fields that encounter strong secondary flows with five-hole pneumatic probes.

2 Fabrication of five-hole probes

The design and fabrication of five-hole pressure probes, in small dimensions, constitute considerably difficult and delicate tasks that require significant expertise. Studies concerning these issues are extremely limited in open literature, contributing further to the difficulties encountered in effective five-hole probe manufacturing. Care has to be taken when soldering the tubes and especially when forming the probe to the desirable shape, in order to avoid tube clogging. In this study,

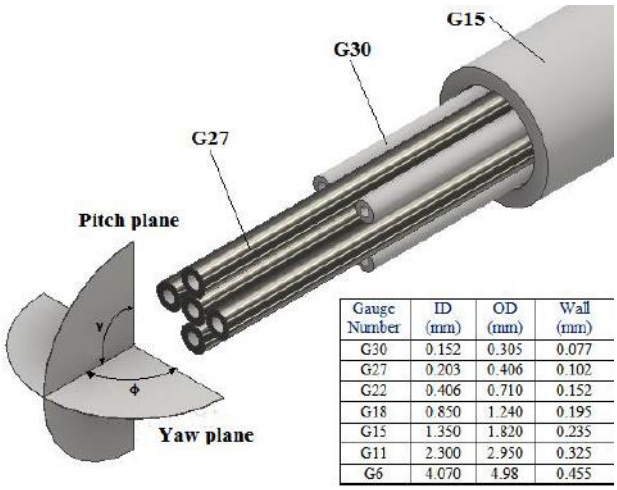

Gauge Number	ID (mm)	OD (mm)	Wall (mm)
G30	0.152	0.305	0.077
G27	0.203	0.406	0.102
G22	0.406	0.710	0.152
G18	0.850	1.240	0.195
G15	1.350	1.820	0.235
G11	2.300	2.950	0.325
G6	4.070	4.98	0.455

Fig. 2. Cross shape maintenance and basic dimensions of stainless steel tubes that were used during construction of the probes

the probes constructed by stainless steel of reported custom made probes [13-16 and 19]. The basic dimensions of the tubes that were used during the construction are illustrated in Fig. 2. The first step made by stacking together 5 hypodermic tubes G27, each with 250 mm length, forming a cross shape. The five tubes were positioned inside a G15 sleeve tube that had a length of 100 mm. Between sleeve tube and G27 tubes were formed gaps, where stainless steel tubes G30 were placed, in order to support and maintain the cross layout (Fig. 2). The combined assembly that left exposed upstream of the sleeve tube was silver soldered to form a solid structure, resulting in an outer tip diameter of D_k = 1.45 mm. Special care was taken to the length that was soldered to minimize the risk of tube clogging. In comparison with the most multi-hole probes, the constructed tip diameter was of sufficient small, though slightly larger than ideal, regarding the outer diameter of the tubes (OD_{id} = 1.22 mm).

The five hypodermic tubes G27 were left exposed and non-soldered downstream of the sleeve tube for a length of 50 mm. Each of them was inserted into stainless steel tubes G22, with 125 mm length, for length extending purposes. Further length extension of the probe reached by fitting

(mm)	Pyramid	Flat
L1	134	120
L2	100	40
L3	40	22
L4	24	15.5
L5	12	8.2
L6	17	17
L7	34	34
Ltot	315	204.5
R1	10.5	14
R2	5.5	7.5
R3	2	1.5
D1	4.98	4.98
D2	2.95	2.95
D3	1.82	1.82
D4	1.45	1.45

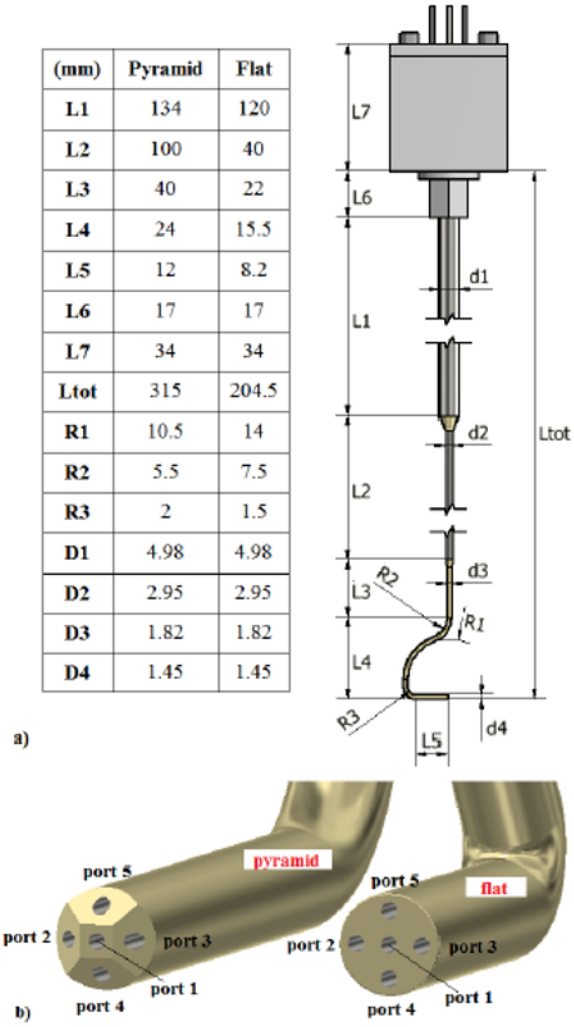

Fig. 3. a) Basic dimensions, b) Head geometries of fabricated five-hole probes

tubes G22 inside of tubes G18 that were 150mm long. All connections were silver soldered to avoid flow leakage. At this stage the flow path was constructed, however the stiffness of the probe was ineffective to resist the aerodynamic forces of the flow, while surface's roughness was unacceptable. In order to handle these, around the tubes G22 and G18 were placed outer tubes G11 and G6 respectively, resulting into great stiffness and surface's smoothness. Fig. 3a illustrates the most significant dimensions of the fabricated probes.

Forming the desirable cobra shape and head geometry constitute the final steps of fabrication. For both probes, the cobra shaping took place in the soldered region and was based on small microdeformations using components of cylindrical surface with different dimensions. As a result, the tip and the cobra shape were of the same miniature diameter of 1.45 mm. In Fig. 3b the threedimensional view of the tip of both five-hole probes is depicted, to clarify the basic difference in head geometry. The tip of the pyramid probe was tapered to an angle of 45º with respect to the longitudinal axis of the central tube, while the tip of the flat probe was non-processed, forming zero angle with respect to the longitudinal axis of the central tube. The tip of the

pyramid probe was made by grinding under a microscope. The dimensions of the probe were extremely small to perform this process with naked eyes. During these final steps, pressurized air was supplied continuously through tubes in order to prevent any buckling or clogging of the tubes.

The cobra shape was selected as it provides an exact known measuring location, given that the tip of the probe is located exactly at the extension of the stem's longitudinal axis. In addition, cobra shape minimizes the flow blockage effect on the local measuring location as the probe's stem is faraway and allows the probe to approach the walls, where boundary layer interactions take place and are of great importance in turbomachinery.

3 Calibration of five-hole probes

3.1 Calibration Setup

The non-nulling calibration method was employed for both five-hole probes in the present study. This type of calibration is widely adopted and requires the pressure probe to be exposed to a steady, uniform flow field of known properties and fixed direction. Inserted in such flow field, the probe is rotated at a previously defined set of angle combinations (pitch [γ] and yaw [φ]) that cover the range of incidence angles that are expected for the probe to encounter during the actual tests. At every angle combination point the pressures of the five holes are measured, resulting into a pressure data matrix from which the calibration and pressure coefficients can be calculated aiming to data reduction.

The calibration process of the pressure probes performed at a small open-type suction wind tunnel, operated with an axial fan installed at the inlet. The tunnel was fabricated by Plexiglas and the exit nozzle's diameter was 80 mm. A honeycomb flow straightener combined with screens was mounted upstream of the exit nozzle, in order to remove any remaining swirl which was induced by the rotor. The test section was an opened working area, where the static pressure was thus atmospheric. The probes were mounted on a calibrated rotating mechanism of high accuracy. The latter mechanism allowed a rotating range of ±34º in both pitch and yaw planes, while the measurement location was fixed. Pressure measurements carried out by using a 16-channel pneumatic pressure scanner that was controlled in proper sequence by a graphical programming environment.

3.2 Calibration and Pressure Coefficients

In open bibliography there are several researchers that have proposed data reduction algorithms, when the calibration is of the nonnulling type [10, 11, 12, and 17]. The major difference among them derives from the magnitude that is used to normalize the coefficients. The choice of this magnitude is of great importance, given the fact that it effects both the angular sensitivity and the range of reliable measurements of the probe.

In this study the convention used to number the five-hole probes is illustrated in Fig. 3b and the calibration coefficients are defined as follows:

Pitch angle coefficient:

$$K_{yaw} = \frac{P_3 - P_2}{P_1 - P_{\alpha v}} \quad (1)$$

Yaw angle coefficient:

$$K_{pitch} = \frac{P_5 - P_4}{P_1 - P_{\alpha v}} \quad (2)$$

Total pressure coefficient:

$$K_t = \frac{P_1 - P_{tot}}{P_1 - P_{\alpha v}} \quad (3)$$

Static pressure coefficient:

$$K_s = \frac{P_{tot} - P_{st}}{P_1 - P_{\alpha v}} \quad (4)$$

where P_{av} is the mean value of the pressures measured by the side holes, that is:

$$P_{\alpha v} = \frac{P_2 + P_3 + P_4 + P_5}{4} \quad (5)$$

Except for the calibration coefficients, the pressures of each hole can be presented as nondimensional pressure coefficients, in order to allow the flow phenomena to be investigated irrespective of the chosen calibration coefficient definitions. The referred individual hole-based pressure coefficients are defined as:

$$Cp_i = \frac{P_i - P_{ref}}{P_1 - P_{\alpha v}} \quad (6)$$

where i represents the identifier of a specific hole between 1 and 5, while P_{ref} is the atmospheric pressure.

3.3 Angular Sensitivity Coefficients

Having the angle coefficients computed by using the equations presented above (1, 2), the evaluation of the probe's ability to identify the variations of the flow angle is feasible. The orthogonal matrices that result from the calibration data can be plotted, as it is illustrated in Fig. 4, in order to provide for each calibration coefficient a surface as a function of angles yaw and pitch. The inclination of the latter surface defines in each angle direction the sensitivity of the calibration coefficient, from which the surface has derived, to the variations of this particular angle.

For each calibration coefficient two angular sensitivity coefficients are computed for each direction as follows:

Yaw sensitivity coefficient:

$$S_{\varphi} = \frac{K_{ref_{i,j+1}} - K_{ref_{i,j}}}{\Delta\varphi} \; for\; i = 1{:}n, for\; j = 1{:}m-1 \qquad (7)$$

Pitch sensitivity coefficient:

$$S_{\gamma} = \frac{K_{ref_{i+1,j}} - K_{ref_{i,j}}}{\Delta\gamma} \; for\; i = 1{:}n-1, for\; j = 1{:}m \qquad (8)$$

where indicator *ref* corresponds to the derived surface, while Δφ and Δγ are the yaw and pitch angle increments respectively.

The values of these coefficients are computed using a double "for" loop sequence. In essence, the uniform grid is scanned at both directions and for each grid point the local value of the surface slope is calculated. In the present study, both angle step increments Δφ and Δγ were equal to 2º in the case of pyramid probe, while they were equal to 4º in the case of flat probe.

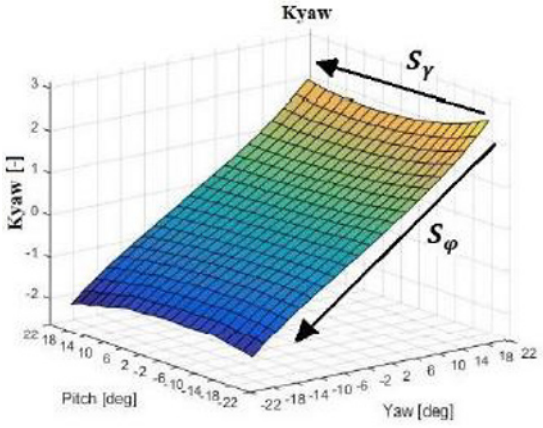

Fig. 4. Coefficient K_{yaw} from pyramid probe, with respect to yaw and pitch angles

4 Calibration results

In the current work, the ideal calibration range for the pyramid probe was about 45º, given the fact that the cone angle was 90º. However, due to the limitations of the rotating mechanism, the calibration range for both the pyramid and the flat probe was set at ±32º in yaw and pitch direction. The angle step increments were different among the two probes. In the case of pyramid probe, the step increments Δφ and Δγ were set at 2º, regarding the yaw (φ) and pitch (γ) angle respectively. As a result a calibration grid of 33x33=1089 points was formed. In the case of flat probe, the step increments were set at 4º, in both yaw and pitch direction, forming a calibration grid of 17x17=289 points. Data were recorded in relatively large time interval Δt of 10 s for each grid point measurement, in order to provide sufficient time to let the pressure waves inside the tubes to settle down, given the fact that the miniature size of the probes increases drastically the time it takes the fluid to

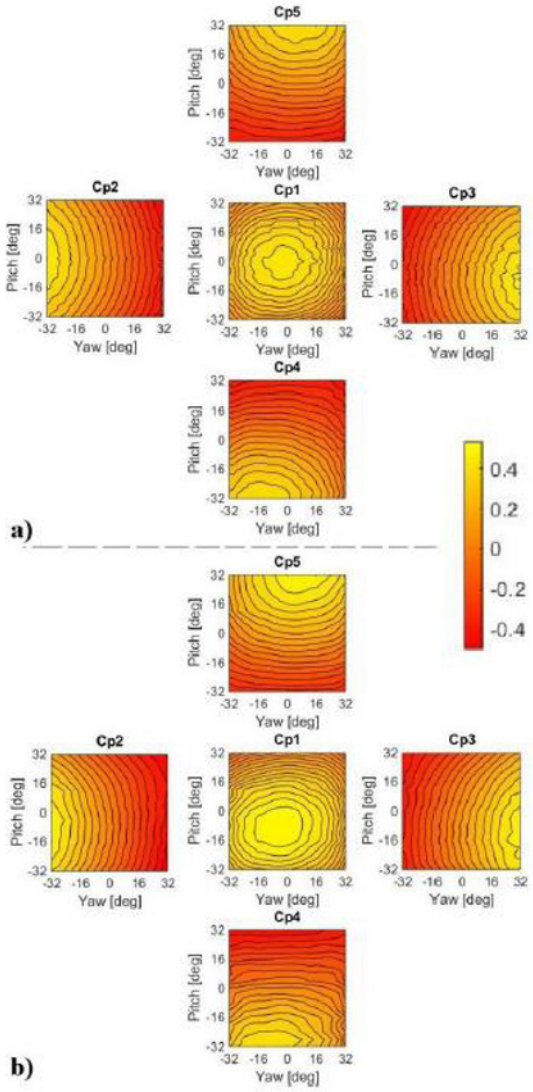

Fig. 5. Non-dimensional pressure coefficient iso-lines from the five ports with respect to yaw and pitch angle a) pyramid probe, b) flat probe

transfer the pressure disturbances through the tubes.

The coefficient equations (5-6) that described previously in this study, were calculated using a mathematical computing software. In Fig. 5 the relationship between the non-dimensional pressure coefficient for each probe port and yaw-pitch angles is illustrated, based on the data provided from the calibration process of each probe. For both probes, the iso-line maps that came out lead to the conclusion that the non-dimensional coefficients for each port are in good agreement with those presented by Morrison et al. [11] and Georgiou and Milidonis [16]. As it was expected, for both pyramid and flat probe, by rotating the probe, the pressure magnitude of each of the four side holes increases as the corresponding port tends to be aligned to the flow direction. The maximum value of the pressure coefficient for the tapered ports, placed at yaw plane, appears at almost 0º pitch angle, while for those placed at pitch plane appears at almost 0º yaw angle. The same behaviour appears for the concentric port that reaches the maximum coefficient value at almost the point of γ=0º

and φ=0º and as the probe is rotated the magnitude of the pressure coefficient decreases. Among the two probes, the pyramid probe shows nearly perfect symmetry, indicating great accuracy in fabrication. The flat probe provides slight misalignment of ports 4 and 5 with respect to the 0º yaw angle. In addition, the pressure coefficient regarding the port 4 of the flat probe, shows some disturbances that may indicate an imperfection of the orifice's edge.

Except for these imperfections, the flat probe is also considered well fabricated with acceptable symmetry, given the fact that a perfectly made custom five-hole probe is hard to obtain, considering a micro scale size. Although the calibration range was set at ±32º for both probes, when analysing the results came out that pyramid probe has a reliable measurement range of ±28º in yaw and pitch direction, while the flat probe has a reliable range of ±24º. For both probes, the measurement uncertainty reduces drastically when the measurement range is limited to ±20º. As a result, this range considered reliable.

As five-hole probe with good performance is excepted to provide accurate measurement of pressure distributions, as well as having good sensitivity in the angular variations of the flow. The latter ability can be evaluated both from the threedimensional surface of the angle calibration coefficients and the angular sensitivity coefficients (7, 8) that described above (Fig. 6, Fig. 7, Fig. 8).

When the probe provides sufficient angular sensitivity, the three-dimensional surface has to be characterized of strong monotonic slope in the direction that the angle coefficient is referred and zero inclination in the opposite direction. Fluctuations on calibration surfaces indicate an inappropriate for measurements coefficient that

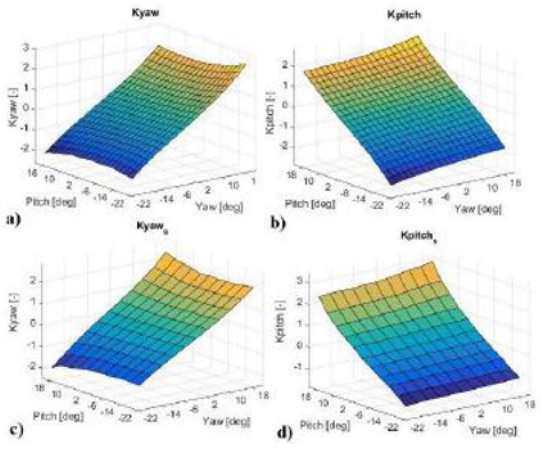

Fig. 6. a) Yaw angle coefficient surface, b) Pitch angle coefficient surface for pyramid probe, c) Yaw angle coefficient surface, d) Pitch angle coefficient surface for flat probe

limits the reliable measurement range. The angular sensitivity coefficients denote monotonic behaviour when they provide explicit positive or negative values, while they denote no sensitivity when are of zero values. In the case of mixed values an inappropriate behaviour is indicated, denoting measurements with increased uncertainty.

The surfaces of the calibration coefficients K_{yaw} and K_{pitch}, regarding the pyramid probe, are presented in Fig. 6a and Fig. 6b, respectively. Both surfaces indicate monotonic behaviour and great smoothness, denoting almost perfect probe fabrication and measurements with high accuracy. In Fig. 6c and Fig. 6d are illustrated the corresponding surfaces regarding the flat probe. Although these surfaces show similar behaviour with those described for the pyramid probe, slight surface declination can be noticed in high positive pitch

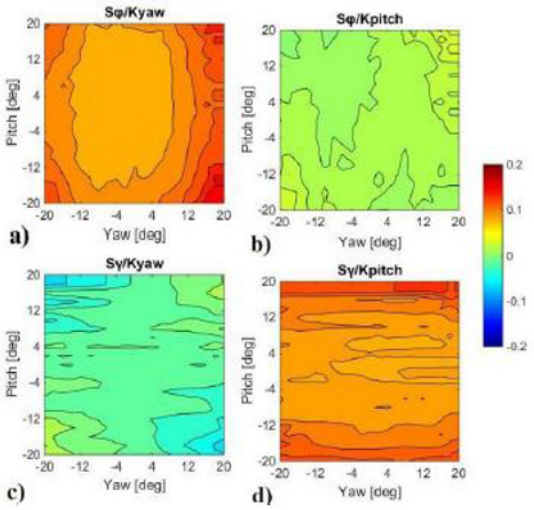

Fig. 7. a) S_φ of K_{yaw}, b) S_φ of K_{pitch}, c) S_γ of K_{yaw}, d) S_γ of K_{pitch} as a function of yaw and pitch angles for pyramid probe

angles for both K_{yaw} and K_{pitch} surfaces. As a result, the flat probe, even though it has non-tapered head geometry, can provide sufficiently accurate measurements in the reliable angle range of ±20º.The contour maps of the angular sensitivity coefficients provided for the pyramid probe are also depicted in Fig. 7.

Regarding the calibration coefficient K_{yaw}, the coefficient S_φ (Fig. 7a) shows explicit positive values, while the coefficient S_γ (Fig. 7c) shows almost zero values all over the angle range. The described behaviour denotes that the magnitude of the yaw angle coefficient is strongly depended on the yaw angle and totally independent of pitch angle. On the other hand, regarding the calibration coefficient K_{pitch}, the coefficient S_φ (Fig. 7b) is now of zero values, while the coefficient S_γ (Fig. 7d) provides explicit positive values. This behaviour denotes that the magnitude of the pitch angle coefficient is strongly depended on the pitch angle and totally independent of yaw angle. Considering these two behaviours together, it can be concluded that pyramid probe has the ability to provide accurate measurements of the flow angles, in the case of being into the reliable range.

In Fig. 8 the contour maps of angular sensitivity coefficients, regarding the flat probe, are presented. The behaviour of each sensitivity coefficient is similar to the

one discussed for the pyramid probe. The only difference can be noticed for coefficient S_γ derived from K_{pitch} coefficient, where in high pitch angles the sensitivity values are highly increased. This phenomenon is in accordance with those described above for the three-dimensional

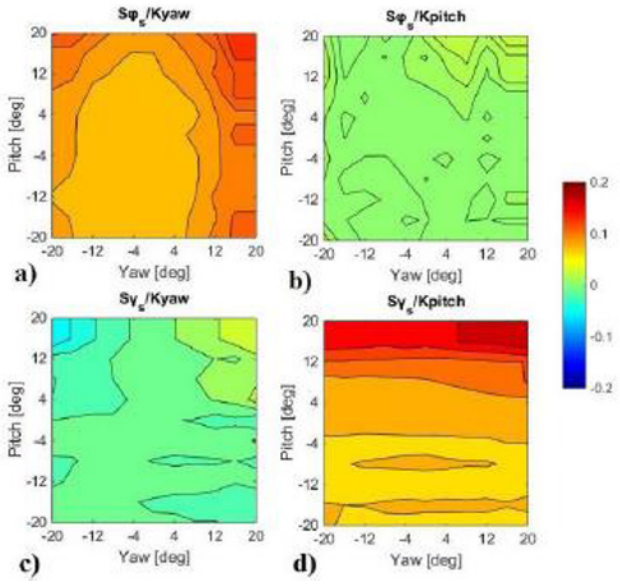

Fig. 8. a) S_φ of K_{yaw}, b) S_φ of K_{pitch}, c) S_γ of K_{yaw}, d) S_γ of K_{pitch} as a function of yaw and pitch angles for flat probe

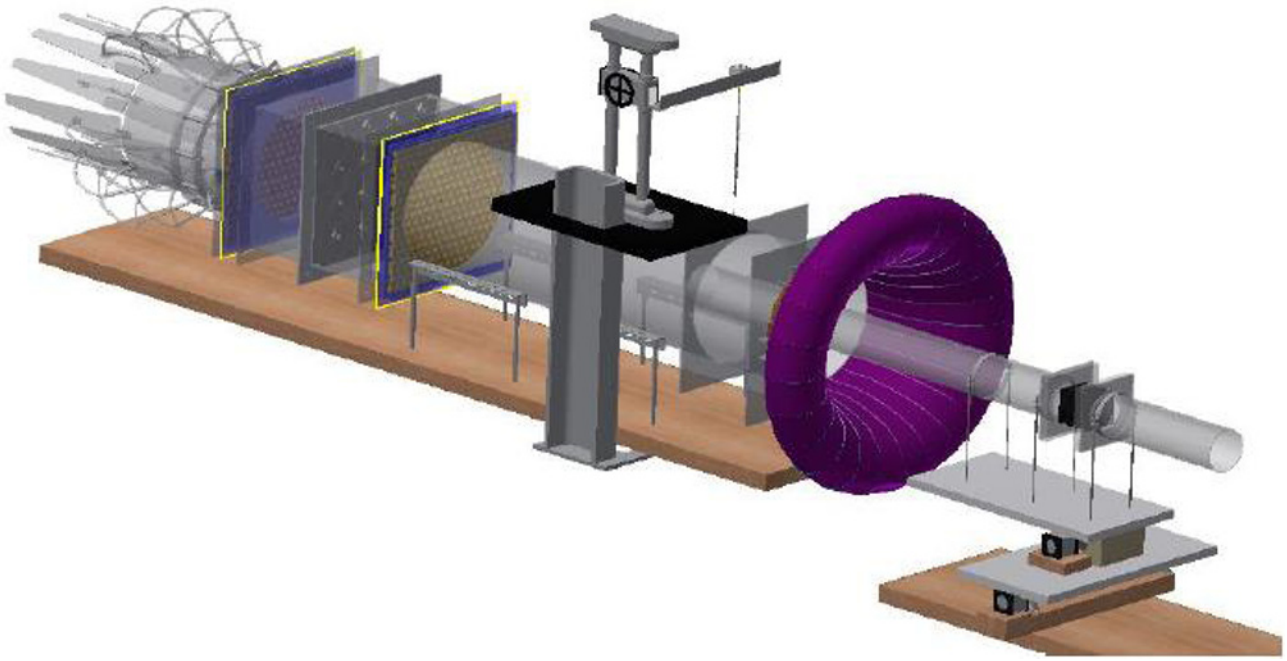

Fig. 9. Experimental setup used for jet in cross flow measurements

surface of K_{pitch} coefficient. Nevertheless, the total angular sensitivity of flat probe is unexpectedly well, given the fact that its tip is totally flat, denoting sufficient accuracy in measuring flow angles.

5 Pyramid probe performance and measurements in jet in crossflow

Taking into account the overall calibration results it can be concluded that pyramid probe is better fabricated than flat probe, as it indicates almost perfect port symmetry, high sensitivity in both yaw and pitch angle variations, totally dissociation of the calibration coefficients and wide angular range of reliable measurements.

As aforementioned, sufficient calibration results were demonstrated for the pyramid probe that indicated the ability to carry out accurate pressure measurements. In order to evaluate the performance of the probe, measurements were obtained in jet in crossflow. Such a flow field, as it is described in numerous studies [21, 22 and 23], encounters strong secondary flows that will demonstrate the proof of operation.

5.1 Experimental setup

The experimental test rig (Fig. 9) is a large-scale model (10:1) of a cylindrical fuel injector, mounted in a two-axis traversing mechanism, which is positioned in an open-type suction wind tunnel calibrated by Vouros et al.[22]. The moving bed allows the rotation and translation of the injector, permitting unconstrained access to measurement planes defined by the researcher. The wind tunnel mass flow is established from a group of sixteen fans positioned parallel, while for the injector from a three stage axially positioned fans. The regulation of the mass flow rates is performed by altering the voltage supplied to the fans, while for the case of the tunnel a variable area nozzle at the exit could be used for the same purpose. Servomotors mounted onthe variable nozzle, control and automate the operation of the experimental rig. The probe was attached on traversing mechanism, able to guide the probe in r direction with high accuracy.

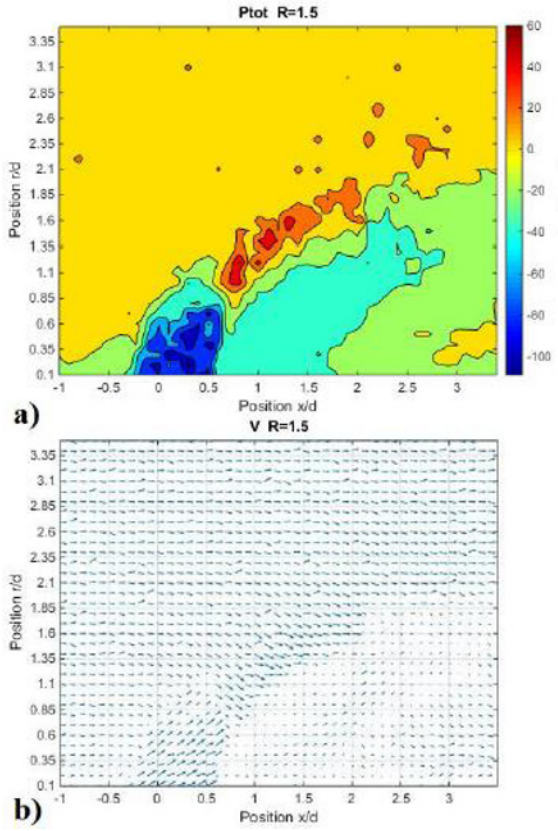

Fig. 10. a) Total pressure iso-lines b) velocity vector distributions in the vertical centre-plane r-x for R=1.5

5.2 Measurements Results

The jet in cross flow measurements conducted for three different velocity ratios (R) in the vertical centre-plane r-x. The ratios investigated were R=1.3, R=1.5 and R=2, while the measurement grid consisted of 35x46=1.610 points. In addition, for the velocity ratio of 1.5, measurements were carried out in three vertical planes r-θ with the distance from the center of the injection orifice to be different. Pressure data from each port were acquired at each grid point by using a 16-channel pneumatic pressure scanner data acquisition system. As for the calibration the time interval Δt of 10 s was employed here too.

Owing to the miniature size of the probe that was of 1.45 mm diameter from the tip to the end of the cobra shape (Fig. 3a), the probe had the ability to approach the injector's wall at a distance of 0.75 mm. This is of great importance when measuring jets in crossflow, as in this region the boundary layer interactions took place and alter the flow mixing. The majority of commercial five-hole probes do not allow very close proximity to the wall, indicating the superiority of the current probe. The measurement results are presented in Fig. 10 in terms of total pressure and velocity distribution, regarding the plane r-x when the velocity ratio is equal to 1.5. The rest of the conducted measurements are not illustrated for the sake of brevity. In Fig 10a, the intense pressure drop in the region above the injection orifice is obvious. In addition, pressure drop is illustrated in the wake region, while in the free stream the pressure losses are of zero values. In Fig. 10b, were the velocity distribution is depicted in terms of velocity vectors, the bend of the jet and the near-field entrainment of main flow fluid that results in the jet break up are observed. The measurements that conducted in the same plane r-x for R=1.3 and R=2 demonstrated that as the velocity ratio increases, the jet penetration, the pressure drop in the region above the orifice and the wake region increase too, while the near-field entrainment of main flow field fluid is reduced. The depicted and described behaviour, is in good agreement with the results provided both with flow visualization [24] and numerical analysis [23], denoting the good performance of the probe, when it is employed in jets in crossflow.

Although the behaviour, provided from the measurements performed with the five-hole probe, shows good agreement with the open literature, the measurements' accuracy is not certain. The uncertainty comes out from the region above the injection orifice, close to the wall level, where the flow is almost perpendicular to the tip of the probe, denoting measurements out of the reliable range. In order to assess the measurements uncertainty, the ideal calibration coefficients were produced and the velocity distributions of the jet in crossflow redefined based on them. The surface fit application of a mathematical computing software was applied to produce the ideal calibration coefficients. As a result, 3^d and 4^{th} order nonlinear polynomial functions produced, regarding the angle and pressure coefficients respectively. The coefficient of determination R^2 was in all the cases greater than 0.99, denoting the good construction of the probe.

The differences between the velocities provided from the ideal calibration map and the ones provided from the raw calibration map were calculated (Fig. 11). Considering that among the two calibration maps the differences are negligible, in the regions of high accuracy, the velocity differences should approach the zero values.

In Fig. 11, the calculated velocity magnitude divergences are presented in a contour plot, regarding the measurements conducted in the plane r-x. The significant divergence in the region above the injection orifice is obvious, denoting that the measurements carried out in this region are not reliable. This uncertainty is expected, given the fact that the flow angle is greater than the reliable range of the probe. In addition, in the wake region, where

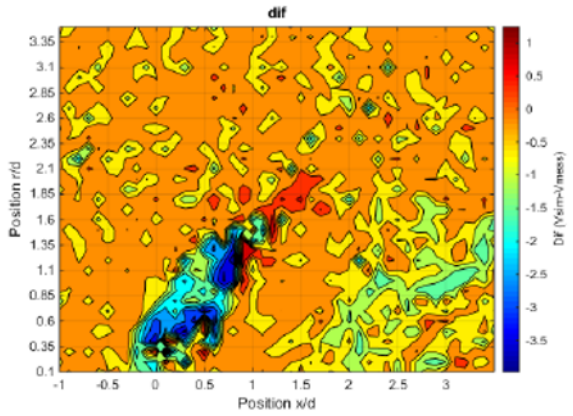

Fig. 11. Contour of Velocity magnitude divergence, among the velocities calculated from the row calibration coefficients and the ones calculated from the ideal coefficients

the secondary flows are intense, some velocity differences of small magnitude are illustrated in the same figure. As a result, in the latter region, the measurements are slightly questionable. In the far field the velocities are of the same magnitude resulting in almost zero divergences that denote reliable measurements.

In overall, although the measurements above the orifice cannot be obtained with extremely high accuracy as the incidence angle is way out of the reliable measurement range, the five-hole probe can provide sufficient measurements in jets in crossflow in order to understand the general behaviour.

6 Conclusions

In the current study, the fabrication and calibration of two different miniature, cobra shape five-hole probes is described. The two probes, provide the same tip diameter of 1.45mm, which is constant till the end of the cobra shape, allowing the probes to approach very close to the solid boundaries. The head geometry was different among the two probes, as the one probe was of pyramid tip that was 45º tapered with respect to the longitudinal axis, while the other one was flat. The effect of this difference was investigated through the calibration results. Haven the calibration procedure completed, the pyramid probe was also implemented in a jet in crossflow, in order to prove the effectiveness of the probe and to evaluate the performance in measuring flowfields with strong secondary flows. The main findings can be summarized in the following section:

- The 5-hole probe with pyramid tip geometry provides efficient calibration results, with reliable measurement range of ±28º in yaw and pitch direction and great angular sensitivity. Uncertainty is reduced at the range of ±20º
- The flat 5-hole probe provides efficient calibration results, justifying the ability to conduct flow measurements with reliable range of ±20º in yaw and pitch direction.
- The miniature dimensions of both probes, allow them to approach a neighbouring solid surface at a distance of just 0.75 mm.
- Flat tip probe provides reliable measurements despite the fact that they are of a very simple form.
- Current optical velocimetry methods compare well with detailed point measurement instruments commonly used in turbomachinery.
- The pyramid 5-hole probe operates reliably in a very large range of constantly changing velocity vector flowfields, such the one appearing in jets in crossflow.

7 Acknowledgments

The authors acknowledge the significant contribution of Alexandros Giannouloudis in the calibration of the flat five-hole probe. We would also like to extend our thanks to S. V. Vouros and A. C. Chasoglou who shared their knowledge on probe manufacturing.

References

1. K. Tanaka, A. I. Kalfas, H. P. Hodson, *Development of Single Sensor Fast Response Pressure Probe*, The XV$_{th}$ Bi-annual Symposium on Measuring Techniques in Turbomachinery Transonic and Supersonic Flow in Cascades and Turbomachines, 21-22 September, Florence, Italy.
2. V. Ramakrishnan, O. Rediniotis, *Development of a 12-Hole Omnidirectional Flow-Velocity Measurement Probe*, AIAA J., **45**, No. 6, pp. 1430-1432 (2007).
3. H. Wang, X. Chen, W. Zhao, *Development of a 17-Hole Omnidirectional Pressure Probe*, AIAA J., **50**, No. 6, pp. 1426-1430 (2012).
4. A. Doukelis, K. Mathioudakis, *Turbomachinery Flow Measurements Using Long-Nose Probes*, GT2003-38488, Proceedings of ASME Turbo Expo, Atlanta, Georgia, USA (June 16-19, 2003)
5. R. G. Dominy, H. P. Hodson, *An investigation of factors influencing the calibration of five-hole probes for three-dimensional flow measurements*, J. Turbomach. Trans. ASME, **115**, pp. 513-519 (July 1993).
6. S. W. Lee, S. B. Jun, *Effects of Reynolds Number on the Non-Nulling Calibration of a Cone-Type Five-Hole Probe,* GT2003-38147, Proceedings of 2003 ASME TURBO EXPO: Power for Land, Sea, & Air, Atlanta, Georgia, USA (June 16-19, 2003).
7. P. C. Ivey, P. D. Smout, *Wall Proximity Effects in Pneumatic Measurement of Turbomachinery Flows*, 94-GT-116 (1994).

8. S. Coldrick, P. C. Ivey, R. Wells, *Considerations for Using 3D Pneumatic Probes in High Speed Axial Compressors*, GT2002-30045, Proceedings of ASME Turbo Expo 2002, Amsterdam, The Netherlands (June 3-6, 2002).
9. A. C. Chasoglou, E. Boufidi, P. Tsirikoglou, A.I. Kalfas, *Novel Multi-hole Pneumatic Probe Geometries for Turbomachinery Application*, The XXII Symposium on Measuring Techniques in Turbomachinery Transonic and Supersonic Flow in Cascades and Turbomachines, France, Lyon (September 4-5)
10. A. L. Treaster, A. M. Yocum, *The calibration and application of five-hole probes*, ISA Transactions, **18**, No. 3 (1979).
11. G. L. Morrison, M. T. Schobeiri, K. R. Pappu, *Five-hole pressure probe analysis technique*, Flow Meas. Instrum., **9**, pp. 153–158 (June 1998).
12. A. J. Pisasale, N. A. Ahmed, *A novel method for extending the calibration range of five-hole probe for highly three-dimensional flows*, Flow Meas. Instrum. 13 (2002), 23–30
13. A. L. Treaster, H. E. Houtz, *Fabricating and calibrating five-hole probes*, Proceedings of the Fluid Measurements and Instrumentation Forum. In: Bajura RA, Billet ML, editors. ASME-Fluids Engineering Division, AIAAiASME 4th Fluid Mechanics, Plasma Dynamics and Lasers Conference, **34**, Atlanta (1986).
14. P. H. Richards, C. G. Johnson, *Development of secondary flows in the stator of a model turbine*, Exp Fluids 1988, **6**, 2–10 (1988).
15. R. Allen, L. Traub, E. S. Johansen, O. K. Rediniotis, T. Tsao, *A MEMS-Based 5-Sensor Probe*, AIAA-2000-0252. Proceedings of the 38th Aerospace Sciences Meeting and Exhibit, Reno, NV (January 10–13 2000).
16. D. P. Georgiou, K. F. Milidonis, *Fabrication and calibration of a sub-miniature 5-hole probe with embedded pressure sensors for use in extremely confined and complex flow areas in turbomachinery research facilities*, Meas. Instrum., **39**, pp.54–63 (2014)
17. D. Telionis, O. Rediniotis, "*Recent Developments in Multi-Hole Probe (MHP) Technology*", Proceedings of COBEM 2009, 20th International Congress of Mechanical Engineering, RS, Brazil (November 15–20 2009).
18. I. Jarallah, V. P. Kanjirakkad, *Improving the fidelity of aerodynamic probes using additive manufacturing*, Rapid Prototyp. J., **22** Iss: 1, pp.200 – 206
19. S. V. Vouros, *Experimental Optimization of a Contra – Rotating Propelling Unit*, Aristotle University of Thessaloniki, Faculty of Engineering, Department of Mechanical Engineering (2015).
20. P. M. Ligrani, B. A. Singer, L. R. Baun, *Miniature five-hole pressure measurement of three mean velocity components in low-speed flows*, J. Phys. E. 1989, **22**, 868–76 (1989).
21. S. V. Vouros, A. C. Chasoglou, T. G. Efstathiadis, A. I. Kalfas, *Effects of Rotor-Speed-Ratio and Crosswind inlet distortion on Off-Design Performance of Contra-Rotating Propelling*, GT2016-57273, Proceedings of ASME Turbo Expo 2016: Turbomachinery Technical Conference and Exposition GT2016, Seoul, South Korea (June 13 – 17 2016).
22. J. Andreopoulos, W. Rodi, *Experimental investigation of jets in a crossflow*, J. Fluid Mech., **138**, pp. 93-127(1984)
23. L. Cortelezzi, A. R. Karagozian, *On the formation of the counter-rotating vortex pair in transverse jets*, J. Fluid Mech., Cambridge University Press, **446**, pp. 347-373 (2001).
24. A. Terzis, Ch. Kazakos, A. Kalfas, P. Zachos, P. Ott, "*Swirl jets in Crossflow at Low Velocity Ratios*", J. Mech. Eng. Autom. 2, pp. 256-266 (2012).